ANALYSIS OF PANDA SPRAY EXPERIMENTS PERFORMED IN TWO INTERCONNECTED VESSELS WITH OpenFOAM

N. Erkan[*], K. Okamoto

Nuclear Professional School, The University of Tokyo
2-22 Shirakata, Tokai-mura, Ibaraki, 319-1188, JAPAN
erkan@vis.t.u-tokyo.ac.jp

ABSTRACT

Containment sprays are one of the accident mitigation systems mix the gas atmosphere and reduce the pressure of the containment in severe accidents of light water reactors (LWRs). While reducing the pressure with the steam condensation, it may create regions with high hydrogen content. For this reason, assessment of spray operations in different gas atmospheres having various thermal-hydraulic properties and gas compositions is essential with the computational codes, which helps to understand the governing mechanisms. PANDA (PSI) experiments addressing the stratified helium gas layer breakup in two interconnected vessels containing steam and steam-air mixtures provide a significant data set for the inter-compartment mass transfer induced by the spray operation for the validation purposes. Numerical codes are very sensitive to the boundary and initial conditions while simulating the transport mechanisms in multivariate scales of tiny droplets and a large nuclear reactor containment. Previous validation studies with a few numerical codes demonstrated large deviations in the predictions of depressurization rates and stratification breakup times. The reasons of such discrepancies could not have been understood sufficiently that might be due to not only related to the modelling techniques but also the uncertainties existed in the experiments. In this paper, we model PANDA spray experiments using an open source computational fluid dynamics code (CFD) OpenFOAM to investigate the depressurization and gas stratification breakup. Owing to the open source character of OpenFOAM, it allows the users to implement problem specific boundary/initial conditions and applications with a higher flexibility. OpenFOAM overestimated the depressurization rates as in the same way of the previous studies. An earlier breakup time of the stratified helium gas layer was predicted; however, transport characteristics between two vessels could be resolved.

KEYWORDS
Containment spray, OpenFOAM, CFD, gas mixing, stratification breakup

1. INTRODUCTION

Containment sprays are one of the emergency devices keeping the containment integrity in the case of light water reactor (LWR) severe accidents. They inject subcooled water into the containment atmosphere, which is filled with condensable and non-condensable gases generated in the reactor core. Injected subcooled water in the form of droplets can cool the containment atmosphere, remove the fission products, and mix the gases preventing excessive local concentrations of hydrogen. The hydrogen generated by the fuel rod cladding oxidation can create locally flammable or even explosive gas mixtures in the LWR containments. When the subcooled water is sprayed into a gas mixture comprised of steam and hydrogen, local hydrogen concentration increases might be encountered because of the steam

removal. For this reason, assessment of spray operations in different gas atmospheres having various thermal-hydraulic properties and gas compositions is essential with the computational codes that provide significant insights about the mechanisms. The interaction of droplets with the surrounding gas poses challenges for the computational codes with respect to the characteristic time and length scales. Extreme difference of spatial scales between the water droplets and the containment building introduce an additional difficulty for resolving the mass/heat exchange phenomena. Accordingly, complex computational efforts are required for a detailed prediction of the relevant physics. Hence, validation of computational codes against large-scale experiments is necessary to predict the post-accident conditions in the containments.

There have been some experimental programs conducted in several large-scale test facilities (TOSQAN, MISTRA, PANDA, and NUPEC) and relevant computational studies to investigate the containment spray effects on the depressurization and the distribution of non-condensable gases. In recent studies, computational codes such as CFX [1], GOTHIC [2] and NEPTUNE_CFD [3] overestimated the rate of gas mixing and could not predict transient evolution of helium-rich layer (simulant gas for Hydrogen) erosion process. That is significant since the alteration in the velocity field, driven by the droplet momentum, and local mixture densities determine primarily the stratified layer erosion and the global redistribution of the non-condensable gases in a complex geometry such as the multi-compartment structure of a real containment building.

Containment sprays also reduce the containment pressure with steam condensation and gas cooling. Depressurization of containment is also important from the aspect of possible pressure induced containment failures. Malet et al. [4] summarized the SARNET spray benchmark results, which include several code's validations against the large-scale experiments. They reported that many computational codes could not predict properly the transient behavior of depressurization even though they could predict the final pressure levels. They also concluded that the main mechanisms of spray depressurization are the heat and mass exchange between the water droplets and gas atmosphere. Mimouni et al. [5] performed a validation study of NEPTUNE_CFD code against PANDA spray tests ST3_0 and ST3_2. NEPTUNE_CFD overpredicted the pressure decrease for the test ST3_2 as in the same way of GOTHIC [2]. They recalculated the pressure variation with the injection of hot water (90 $^{\circ}$C) for an initial 100 s period considering that injection pipe was hot initially. The obtained pressure variation approached to the experimental one; however, depressurization was still faster than the experiment. Although that was the case, how long a hot injection pipe can maintain the water temperature at 90 $^{\circ}$C during 100 s is open to discussion, and we think that other mechanisms must play significant roles, which still need to be investigated.

PANDA experiments (ST3_1 and ST3_2) [6] with an initial Helium layer in one vessel provide significant data about the transient pressure response to the spray activation, the breakup of the stratified helium-rich layer, and the time-dependent distribution of the non-condensable gas within the compartments. Moreover, two interconnected vessel geometry is very important in terms of the possibility of potentially dangerous hydrogen mixtures formation in regions far away from the spray.

Numerical codes are very sensitive to the boundary and initial conditions while simulating the transport mechanisms in multivariate scales of tiny droplets and a large nuclear reactor containment. Previous validation studies with the CFD or lumped parameter (LP) codes demonstrated large deviations in the predictions of depressurization rates and stratification breakup times. The reasons of such discrepancies could not have been understood sufficiently that might be due to not only pertinent to the modelling techniques but also the uncertainties existed in the experiments. In this paper, we model PANDA (ST3_1 and ST3_2) spray experiments using an open source CFD code – OpenFOAM - to investigate the depressurization and gas stratification breakup in the PANDA spray experiments. Owing to the open source character of OpenFOAM, it allows us to implement the test specific boundary/initial conditions

and applications with a higher flexibility. With the help of that ease experimental droplet size distributions are implemented as a new size distribution model in the source code. Besides this, a condensation model is also adopted.

2. OpenFOAM AND NUMERICAL MODEL

OpenFOAM is an open source parallel CFD code. It contains various solvers to simulate complex fluid flows including dispersed two phases such as sprays. OpenFOAM solves the transport equations with finite volume method in 3D unstructured mesh. In this study sprayFOAM solver is employed for the 3D simulation of the spray operation in PANDA vessels. Originally, sprayFOAM was developed for engine fuel sprays and it can only calculate the evaporation from the fuel droplets. Here, relevant condensation models and heat transfer models are implemented into the source code to simulate the steam condensation/evaporation on the water droplets.

2.1. Governing equations

OpenFOAM solves the dispersed phase equations with Lagrangian approach and carrier gas phase transport equations with Eulerian approach. Two phases coupled with each other in terms of mass, momentum and energy transfers. The unstructured 3D mesh is used to discretize the conservation equations of the gas phase.

Mass transfer equations:

$$\frac{\partial \rho}{\partial t} + \nabla \cdot (\rho U) = \dot{\rho}_s \tag{1}$$

Equation 1 formulates the total mass balance for the gas phase. Where, ρ is the density, t is the time, U is the velocity. $\dot{\rho}_s$ is the source term which is calculated from the condensation on the droplets or evaporation from the droplets. Each species in the gas phase are transported by diffusion and convection, and only steam is consumed or produced by the condensation or evaporation respectively. Mass transport for the individual species in the gas phase is as follows;

$$\frac{\partial \rho Y_i}{\partial t} = \nabla \cdot (\rho U Y_i) - \nabla \cdot (\mu_{eff} \nabla Y_i) = \dot{\rho}_s^i, \quad \dot{\rho}_s = \sum_i \dot{\rho}_s^i \tag{2}$$

where, Y_i is the mass fraction of ith specie. $\mu_{eff} = \mu + \mu_T$ is the sum of laminar and turbulent viscosities. Here, source term is nonzero for only the steam.

Momentum transfer equation:

$$\frac{\partial \rho U}{\partial t} + \nabla \cdot (\rho U U) = -\nabla p + \nabla \cdot (\mu_{eff} \nabla U) + \nabla \cdot [dev(\mu_{eff}(\nabla U)^T)] + \rho g + F_s \tag{3}$$

where, p is the pressure, g is the gravitational acceleration, F_s is the momentum source term induced by the spray droplets. dev returns the deviatoric part of a symmetric tensor defined as $dev(A) = A - \frac{2}{3} Itr(A)$.

Energy transfer equation:

$$\frac{\partial \rho(h+K)}{\partial t} + \nabla \cdot (\rho U(h+K)) - \frac{dp}{dt} - \nabla \cdot \alpha_{eff} \nabla h = H_s \tag{4}$$

Energy transport is solved with enthalpy equation since the gas phase treated as compressible in the solver. In Equation 4, h and K denote the specific enthalpy and specific kinetic energy respectively. α_{eff} is turbulent thermal diffusivity. H_s is the heat source or sink term which gives the heat exchange between the droplets and gas phase.

Water droplets are assumed to have sphere shapes. Motion of droplets is treated with Lagrangian approach. The momentum equation for the droplets is written as;

$$\frac{\partial P_d}{\partial t} = -\rho_g \frac{\pi d^2}{8} C_D (u_d - U)|u_d - U| + \rho_d \frac{\pi d^3}{6} g \tag{5}$$

In Equation 5, only drag and gravity force effect the particle motion. C_D is the drag coefficient for spherical particles. u_d and d refer the droplet velocity and droplet diameters. ρ_d is the droplet density. Droplet diameter variation during their flight is considered as small so that it is assumed not to alter the drag and gravity force.

Mass and heat transfer on the droplets interfaces are calculated using following equations and correlations;

$$\frac{dm_d}{dt} = \pi d Sh D_{ab} \rho_{vs} \, log[1 + X_r] \qquad X_r = \begin{cases} \frac{X_{v,\infty} - X_{v,s}}{1 - X_{v,s}}, & X_{v,s} < X_{v,\infty} \\ \frac{X_{v,s} - X_{v,\infty}}{1 - X_{v,s}}, & X_{v,s} > X_{v,\infty} \end{cases} \tag{6}$$

$$Sh = 2 + 0.6 Re_d^{1/2} Sc^{1/3} \tag{7}$$
$$Nu = 2 + 0.6 Re_d^{1/2} Pr^{1/3} \tag{8}$$

where, m_d is the droplet mass, $X_{v,\infty}$ and $X_{v,s}$ are the steam mole fractions in the gas phase and near the droplet surface respectively. Sh is the Sherwood number, Re_d is the droplet Reynolds number. Schmidt number defined as $Sc = \vartheta/D_{ab}$, where, ϑ is the kinematic viscosity. Nu and Pr are the Nusselt and Prandtl numbers respectively.

2.2. Initial and Boundary conditions

Experiments do not include information about the droplet injection velocities. In reality, we assumed that droplet velocities take terminal velocities in a short time after the injection and in a short distance compared to the scale of the vessel. Considering the experimental Sauter mean diameter and terminal velocity, droplet injection velocities were fixed at 6 m/s. Droplets were generated and injected with 30° cone angle randomly according to the log-normal size distribution function provided by Erkan et al. [6]. 2000 parcels were injected in a second to represent the droplets.
Initial helium layer was set as similar to the experiment, which has non-uniform helium layer with a concentration gradient region. The gradient region was imitated with a linear concentration distribution function reproduced from the experimental initial conditions.
Injection temperature and flow rate were the same for both tests. Vessel walls were taken as adiabatic boundary. Initial pressure and temperature were taken as the nominal values presented in [6]. k-epsilon turbulence model was applied to the gas phase.

3. EXPERIMENTAL SETUP

Two experiments were performed in the PANDA facility with different gas compositions. Erkan et al. [6] reported details of both experiments. The tests named as ST3_1 and ST3_2 utilized two interconnected vessels. Nominal values of initial and boundary conditions are shown in Figure 1. The tests started with subcooled water injection with the temperature of 40 °C at a constant flow rate of 0.84 kg/s from 6.9 m height. Helium-rich layer were formed initially. Helium concentration in the layer was not constant along the vertical axis. Gas concentrations were measured at some positions in vessel system, which are shown in Figure 2.
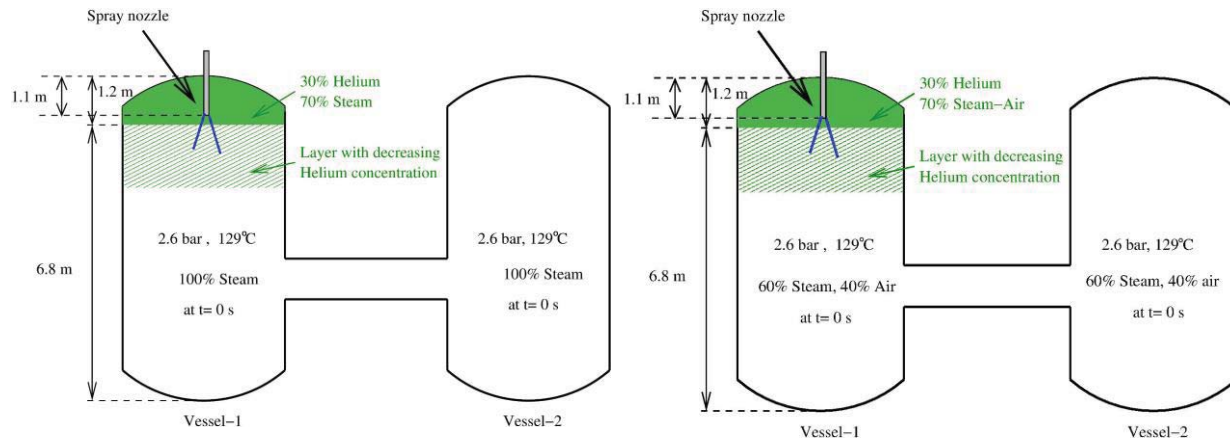
Figure 1. Initial conditions for the test (a) ST3_1 and (b) ST3_2 [6].
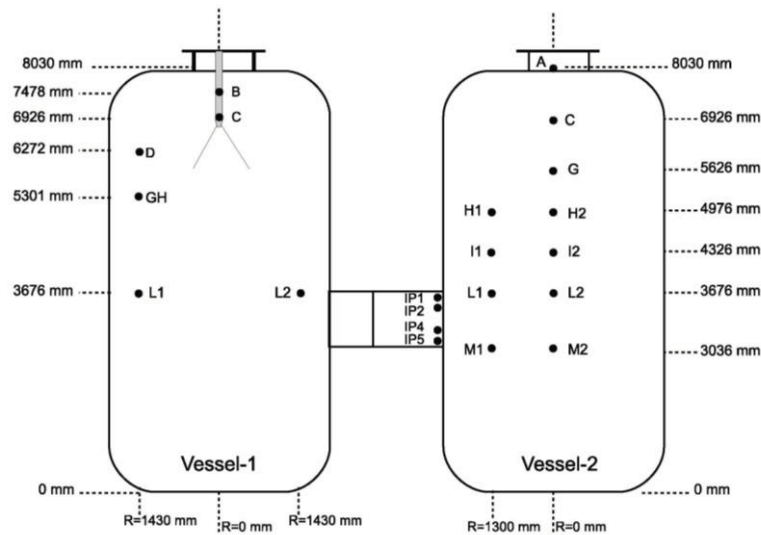
Figure 2. Gas concentration measurement locations in a vessel and interconnecting pipe (IP) [6].

4. RESULTS AND DISCUSSIONS

4.1. Depressurization

Spray injection starts at time *t=0* and continues until the end of the test. Numerical and experimental non-dimensional pressure variations are compared in Figure 3 for both cases. Depressurization rate is overpredicted for both tests. The deviation between the simulation and experiment is larger in the case of ST3_1 that is likely to be because of the higher steam composition of the test. That larger discrepancy

implies a direct relation of depressurization with condensation rate, in another word, mass exchange between the droplets and gas atmosphere. Since the non-condensable gas content is higher in ST3_2, simulation result does not diverge from the experiment as much as it does in ST3_1.

 Andreani and Erkan [2] obtained the similar tendencies for the pressure variations in their validation studies. They investigated the reasons of those large discrepancies with enhancement of heat transfer coefficient from the walls. The results were improved to some extent; however, depressurization rate was still remarkably higher in the simulation. They concluded that, heat transfer from the walls could be a reason; however, overprediction of condensation might contribute to too fast depressurization.

Mimouini et al. [5] also found the discrepancies in the depressurization rates for the test ST3_2. They performed a sensitivity analysis by changing the droplet diameters and water injection temperatures. They observed that depressurization rate was not affected by the droplet diameters. On the other hand, 90 °C water injection during the first 100 s improved the simulation results. Although elevated temperature in the water injection was an assumption, we do not agree with that assumption, that analysis demonstrates that heat, and mass transfer between the gas atmosphere and droplets possibly play a major role in the depressurization. Further sensitivity analyses concentrating on the exchange phenomena are needed to resolve the modelling discrepancies.
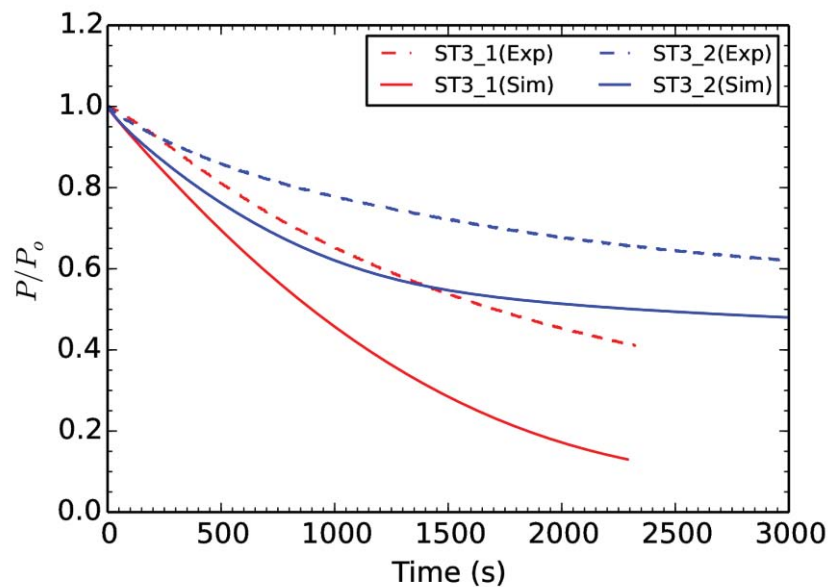
Figure 3. Pressure variation with time (P_o: initial pressure).

4.2. Gas mixing

Spray induces mixing in the containment atmosphere by mechanical interactions of droplets with the gas phase. Figure 4 presents the calculated and experimental Helium molar fraction variations are normalized with initial helium molar fraction (X_{He}^B) at position B. In the test ST3_1, the numerical simulation predicts a rapid helium erosion in 150 s (Figure 4a). However, in the experiment, erosion process continues until 400 s. Additionally, the initial rapid increase of the helium fraction cannot be captured with the simulation. The reason of this initial peak in the test is not clear, however, it was likely originated from the proximity of the measurement location to the injection pipe on which rapid condensation took place with the onset of cold water injection. Because of that rapid increase in the Helium concentration, layer erosion might have taken longer time. After the mixing, helium concentrations converge to the same level in the experiment and the simulation. By the time elapses, helium fractions increase faster than the

experiment that might be because of the overprediction in steam condensation rate on the droplets. Helium concentration increases at the middle of the vessel in agreement with the experimental result (position L1 in Figure 4a). The Increasing tendency of concentration is also observed at position L1 because of the overprediction of steam condensation.

For the test ST3_2, similarly a faster mixing time is predicted compared to the experiment. Contrarily, helium fractions converge to same asymptotic level with the experiments since initial steam fraction is lower than the test ST3_1 and the depletion rate of total gas inventory is slower.

Helium-rich layer stratification breakup and erosion is highly related to the global flow induced by the spray droplets. Although the simulation could not predict the timings of the breakup and erosion properly, an apparent delay can be observed between the two test cases. In particular, numerical simulation predicts the mixing times as $t=100$ s for ST3_1 and as $t=200$ s for ST3_2. Figure 5 illustrates flow vectors for both test cases at $t=100$ s. At first sight, differences in the flow patterns in the helium-rich region can be observed. For the test ST3_1 flow vectors at around and slightly above the spray injection level are mostly directed to downward directions with larger vertical components, while they are aligned horizontally around the injection level in the case of ST3_2. These results demonstrate that surrounding gas is entrained downward direction more strongly in higher steam fraction gas environment, which is directly related to the rapid depletion of steam with condensation in test ST3_1. On the other hand, lower rate of steam depletion encountered in ST3_2 because of higher non-condensable gas concentration does not create strong entrainment as much as it does in ST3_1.
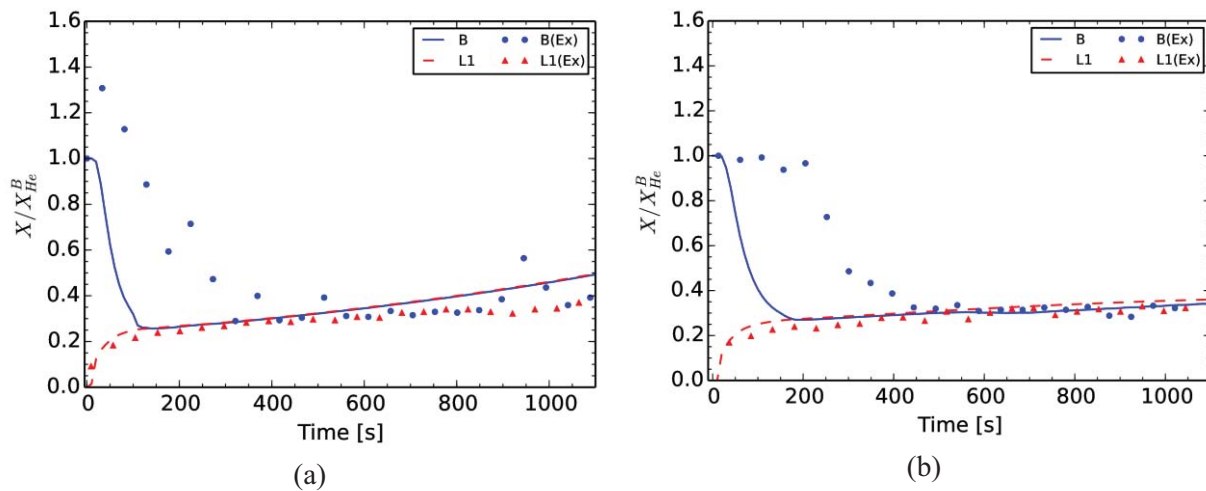
Figure 4. Helium molar fraction variations in Vessel-1, (a) ST3_1, (b) ST3_2.
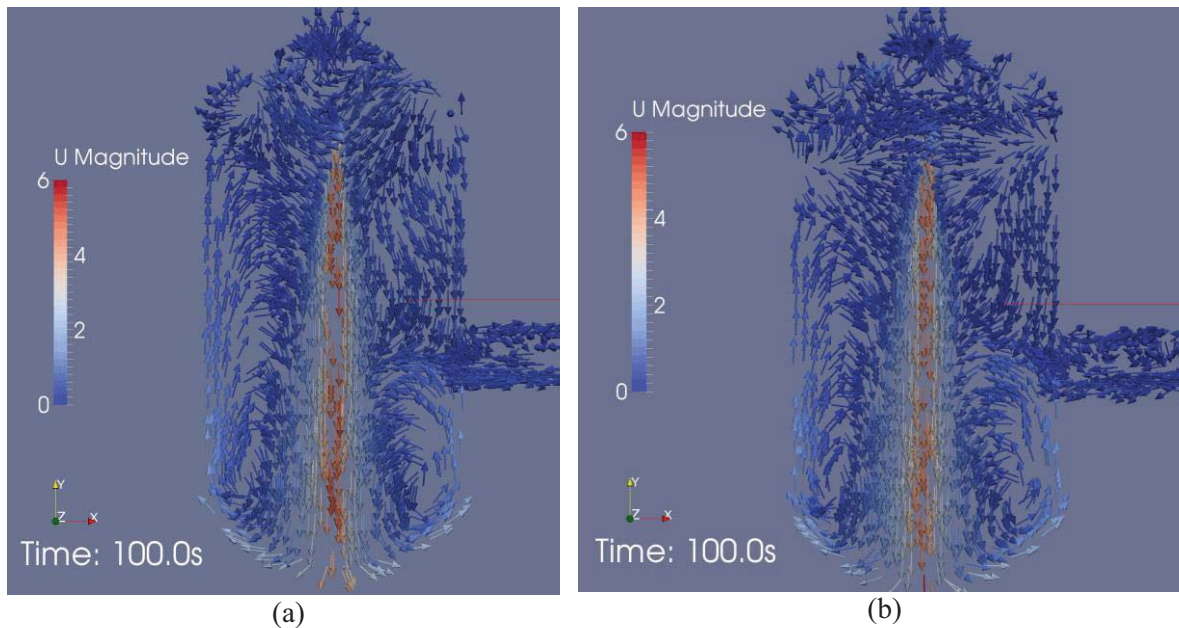
Figure 5. Velocity vectors at *t=100 s* in Vessel-1, (a) ST3_1, (b) ST3_2. Velocity magnitude unit is m/s.

Gas transport through the interconnecting pipe (IP) between the vessels is induced by the spray operation. Helium-rich gas mixture in Vessel-1 moves to the Vessel-2. After the steam condensation started, the density of the gas mixtures changes depending on the fractions of species. Figure 6 shows calculated non-dimensional helium molar fraction variations in Vessel-2 compared with the experimental data. In contrast to the earlier breakup predictions of helium layer, which is expected to induce rapid transfer of helium to Vessel-2, increase of helium concentrations in the Vessel-2 delay in time relative to the experimental results. In ST3_1 calculations, helium concentration levels exceed the experimental values later in time (Figure 6a). Inversely, helium concentrations remain lower than the experimental levels for test ST3_2 (Figure 6b). Erkan et al. [6] presented density variations at the measurement positions and concluded that density variations due to condensation and cooling determines the characteristics of bidirectional gas transfer between the vessels. Based on that argument, large discrepancies in the Vessel-2 helium concentration predictions can be regarded as reasonable under the consideration of disagreements in the pressure calculations (Figure 3).

Nonetheless, transport characteristics of the helium-rich mixture agrees with the experiments due to the reasons proposed in [6] and as can be seen from the helium mass fraction contour maps in Figure 7. In the test ST3_1, reduction of the steam content in the helium-steam gas mixtures generates a lighter gas composition and it flows towards the Vessel-2 via the upper region of IP and move upward inside Vessel-2 (Figure 7a). At the same time, heavier steam-rich gas mixture coming from Vessel-2 descends towards the bottom plenum of Vessel-1.

For the test ST3_2, an opposite situation is observed (Figure 7b). Condensation of steam leaves behind a heavier gas mixture in the helium-steam-air gas composition contrary to the helium-steam mixture. Owing to higher density, helium-rich mixture travels through the lower side of the IP and descend towards the bottom plenum of Vessel-2. In the mean time, flow stream coming from the Vessel-2 rise upward in the Vessel-1.
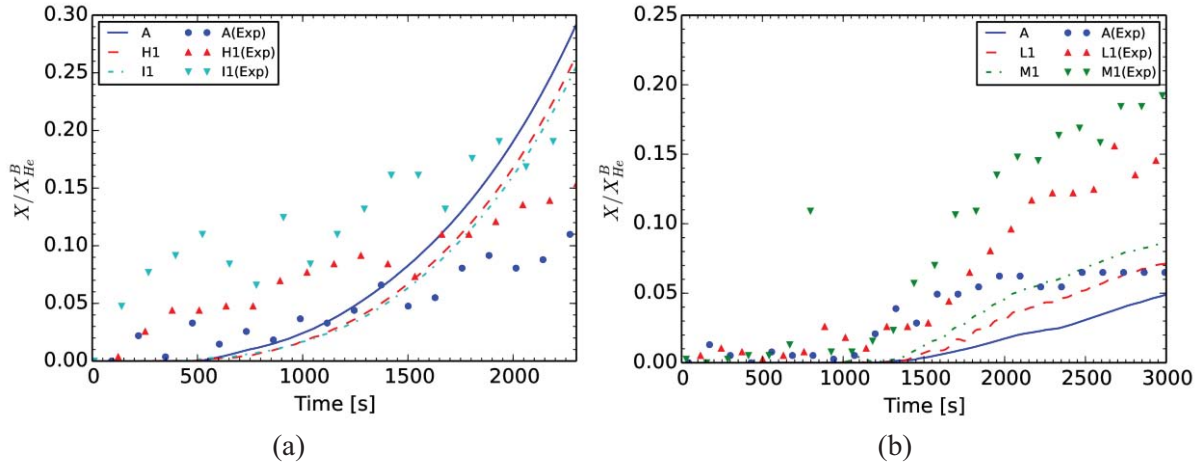
Figure 6. Helium molar fraction variations in Vessel-2, (a) ST3_1, (b) ST3_2.
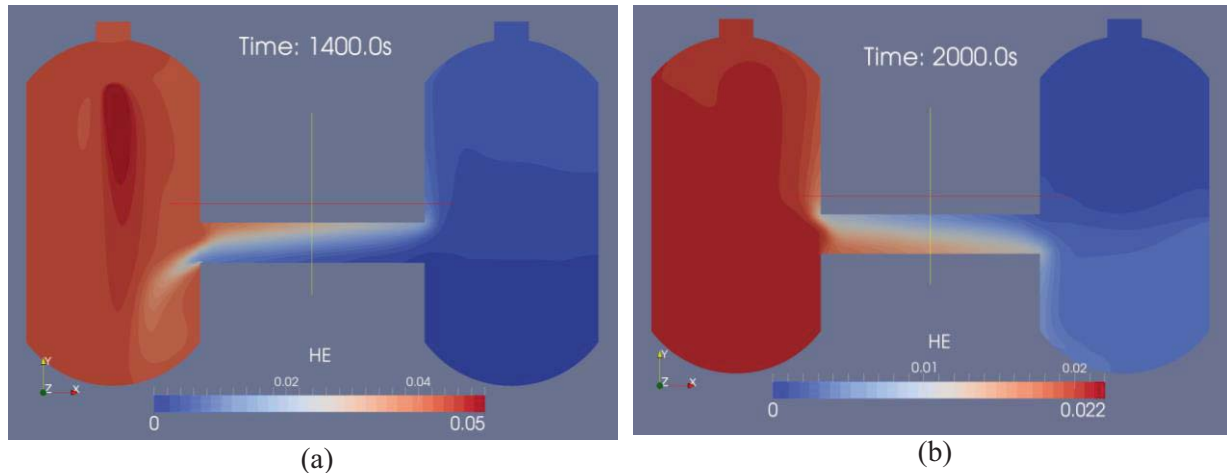
Figure 7. Helium mass fractions (a) ST3_1, (b) ST3_2.

5.   CONCLUSIONS

Subcooled water spray operation was simulated with OpenFOAM for the tests performed in the interconnected vessel system of PANDA facility. The results were compared with the tests ST3_1 and ST3_2. Both tests had initial helium-rich layer in one vessel in which a spray operated in whole duration of the experiment.

Depressurization rates were overestimated, which was the most common problem encountered in previous validation studies performed with other codes in the literature. The reason of such big differences in the depressurization rates is likely to be originated from the steam condensation rates on the droplets in a non-condensable gas mixture environment. Although some other reasons pertinent to the initial and boundary conditions of the experiments were considered previously, they are still needed to be investigated.

In the simulation, helium-rich layer breakup and erosion times were predicted faster than the experiment. That discrepancy might also be originated from the problems relevant to interfacial mass exchange on droplet surfaces.

Flow patterns around the spray in the helium-rich layer demonstrates different behaviors for tests, which is probably the major mechanism governing the helium-rich layer erosion.

Some differences were also observed in the helium concentration variations in Vessel-2 which is far away from the spray. Helium-rich mixture was transported to Vessel-2 through the IP. Rate of increase in the helium concentrations was underestimated. Even this is the case; differences of helium-rich mixture flows in the vessel system could be resolved.

Further investigations are needed to examine the large differences between the simulation and experiments.

REFERENCES

1. M. Babic, I. Kljenak, B. Mavko, "Simulations of TOSQAN containment spray tests with combined Eulerian CFD and droplet-tracking modelling," *Nucl. Eng. Des.* **239**, pp. 708–721 (2009).
2. M. Andreani, N. Erkan, "Analysis of spray tests in a multi-compartment geometry using the GOTHIC code," *Proc. of 18th Int. Conf. on Nucl. Eng. (ICONE18)*, Xi'an, China, May 17–21 (2010).
3. S. Mimouni, J. –S. Lamy, J. Lavieville, S. Guieu, M. Martin, " Modelling of sprays in containment applications with a CMFD code," *Nuc. Eng. Des.* **240**, pp. 2260-2270 (2010).
4. J. Malet, L. Blumenfeld, S. Arndt et al. "Sprays in containment: Final results of the SARNET spray benchmark," *Nuc. Eng. Des.* **241**, pp. 2162-2171 (2011).
5. S. Mimuoni, C. Baudry, A. Douce et al., "Modelling of sprays in a multi-compartment geometry with a CMFD code," *Proc. of 15ᵗʰ Int. Topical Meeting on Nuclear Reactor-Thermal-Hydraulics (NURETH-16)*, Pisa, Italy May 12-17 (2013).
6. N. Erkan, R. Kapulla, G. Mignot et al., "Experimental investigation of spray induced gas stratification break-up and mixing in two interconnected vessels," *Nuc. Eng. Des.* **241**, pp. 3935-3944 (2011).